PHYSICAL REVIEW E **96**, 061102(R) (2017)

Relative velocities in bidisperse turbulent suspensions

J. Meibohm, L. Pistone, K. Gustavsson, and B. Mehlig
Department of Physics, Gothenburg University, SE-41296 Gothenburg, Sweden
(Received 5 March 2017; revised manuscript received 18 July 2017; published 14 December 2017)

We investigate the distribution of relative velocities between small heavy particles of different sizes in turbulence by analyzing a statistical model for bidisperse turbulent suspensions, containing particles with two different Stokes numbers. This number, St, is a measure of particle inertia which in turn depends on particle size. When the Stokes numbers are similar, the distribution exhibits power-law tails, just as in the case of equal St. The power-law exponent is a nonanalytic function of the mean Stokes number $\overline{\mathrm{St}}$, so that the exponent cannot be calculated in perturbation theory around the advective limit. When the Stokes-number difference is larger, the power law disappears, but the tails of the distribution still dominate the relative-velocity moments, if $\overline{\mathrm{St}}$ is large enough.

DOI: 10.1103/PhysRevE.96.061102

I. INTRODUCTION

The dynamics of small heavy particles in turbulence plays a crucial role in many scientific problems and technological applications. Any model of the particle dynamics must refer to the turbulence the particles experience. This is a challenge for realistic modeling of such systems, for their direct numerical simulation (DNS), and for experiments. Novel particle-tracking techniques and improved DNS algorithms have made it possible to uncover striking phenomena in turbulent aerosols. For example, heavy particles tend to avoid the vortices of the turbulent fluid, and they form small-scale fractal patterns. Nearby particles can have very high relative velocities, an effect caused by "caustic" singularities in the particle dynamics. The analysis of statistical models has led to substantial progress in explaining these phenomena, reviewed in Ref. [1]. This analysis has offered fundamental insights about how caustics shape the distribution of relative velocities of nearby particles [2–10].

These results apply only to "monodisperse" suspensions of *identical* particles. An important question is therefore how particles of *different* sizes cluster and move relative to each other. Spatial clustering of such "bidisperse" suspensions was analyzed in Refs. [11,12]. The particles cluster onto two distinct attractors, and the fractal distribution of separations between differently sized particles is cut off at a small spatial scale, r_c, that can be much larger than the particle size.

Here we analyze the distribution of relative velocities of particles with different sizes. Our results are important for the physics of turbulent aerosols, because the distribution of relative velocities determines the relative speeds of colliding particles, their collision rate, and collision outcomes [13–16].

In a dilute suspension of small, heavy, spherical particles the dynamics of a single particle is approximately given by Stokes law with constant $\gamma \equiv 9\rho_f \nu/(2a^2\rho_p)$:

$$\frac{d}{dt}\boldsymbol{x} = \boldsymbol{v}, \qquad \frac{d}{dt}\boldsymbol{v} = \gamma[\boldsymbol{u}(\boldsymbol{x},t) - \boldsymbol{v}]. \tag{1}$$

Here $\boldsymbol{x}$ and $\boldsymbol{v}$ are particle position and velocity, a is the particle size, ν is the fluid viscosity, and ρ_f and ρ_p are fluid and particle densities. We model the turbulent fluid velocities by a random Gaussian velocity field $\boldsymbol{u}(\boldsymbol{x},t)$ with zero mean, correlation time τ, correlation length η, and typical speed u_0, representing the universal small spatial scales of turbulence [17], neglecting intermittent, non-Gaussian features [1]. It has been shown that many important features of the dynamics of heavy particles in turbulence are explained by this model [1]. Equation (1) assumes that the particle and shear Reynolds numbers are small. Gravitational settling [18–22] is disregarded; this is valid when the turbulence is intense enough. The dimensionless parameters of the model are the Stokes number $\mathrm{St} \equiv 1/(\gamma\tau)$, a measure of particle inertia, and the Kubo number, $\mathrm{Ku} \equiv u_0\tau/\eta$, measuring the persistence of the flow.

II. RELATIVE VELOCITIES

Figure 1(a) summarizes results of statistical-model simulations in two spatial dimensions, for the distribution $\varrho(v_r,r)$ of relative radial velocity v_r and separation r between particles with slightly different Stokes numbers. Color coding and the black isolines in Fig. 1(a) are logarithmic. As a consequence, regions of equidistant isolines correspond to power laws. Figure 1(a) thus shows that the distribution exhibits a power-law tail as a function of r for small v_r and becomes uniform for small r. The crossover between the tail and the plateau defines the cut-off scale r_c, observed and discussed in Refs. [11,12].

Furthermore, Fig. 1(a) shows that there is a second cut-off scale, v_c, that distinguishes between a power law as a function of v_r for large v_r, and a plateau for small v_r. Our numerical results demonstrate that this new scale v_c does not depend on r [Fig. 1(a)]. This is in marked difference to the monodisperse case, where the distribution has no plateau in the limit of $r \to 0$. Panel (b) shows that v_c depends linearly on the parameter $\theta \equiv |\mathrm{St}_1 - \mathrm{St}_2|/(\mathrm{St}_1 + \mathrm{St}_2)$ measuring the difference between the Stokes numbers. Panel (c) shows distributions for $r \ll r_c$ as functions of v_r, for different values of θ. The dashed line is the power law $|v_r|^{\mu_c - d - 1}$, where $d = 2$ is the

Published by the American Physical Society under the terms of the Creative Commons Attribution 4.0 International license. Further distribution of this work must maintain attribution to the author(s) and the published article's title, journal citation, and DOI.

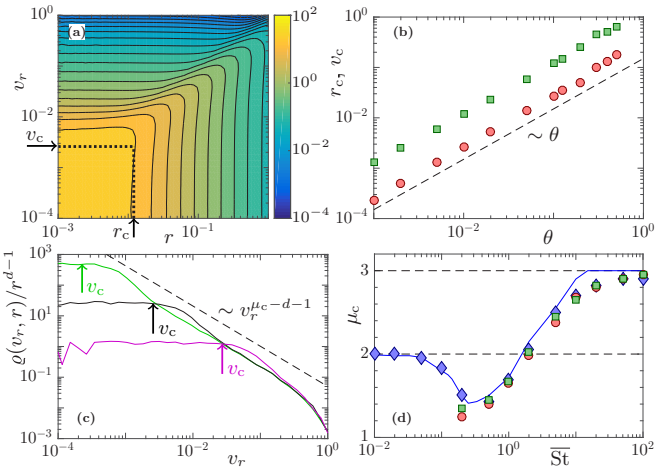

FIG. 1. Distribution $\varrho(v_r,r)$ of relative velocities between particles with different Stokes numbers. Statistical-model simulations in two dimensions ($d=2$) for $\mathrm{Ku}=1$. (a) Contour plot of $\varrho(v_r,r)/r^{d-1}$ for $\overline{\mathrm{St}}=1$ and $\theta=10^{-2}$ (see text). Dotted lines show cut-off scales r_c and v_c. (b) Dependence of r_c on θ (green $\square$), and of v_c on θ (red $\circ$), for $\overline{\mathrm{St}}=1$. (c) $\varrho(v_r,r)/r^{d-1}$ evaluated at $r<r_c$, for $\overline{\mathrm{St}}=1$ and $\theta=10^{-3}$ (green line), $\theta=10^{-2}$ (solid black line), and $\theta=0.1$ (magenta line). Crossover scales v_c (arrows). (d) Power-law exponent μ_c versus $\overline{\mathrm{St}}$ for small θ. Exponent for power-law tails in v_r for fixed r with $\theta=10^{-3}$ (green $\square$) and $\theta=10^{-2}$ (red $\circ$). Exponent for power-law tails in r for fixed v_r with $\theta=10^{-2}$ (blue $\diamond$). Numerical data for $\min(D_2,d+1)$ where D_2 is the phase-space correlation dimension (solid blue line).

spatial dimension. Panel (d) demonstrates that the exponent μ_c is approximately equal to $\min(D_2,d+1)$ where $D_2(\overline{\mathrm{St}})$ is the phase-space correlation dimension of a suspension of identical particles with Stokes number $\overline{\mathrm{St}}\equiv(\overline{\gamma}\tau)^{-1}$ and $\overline{\gamma}=\frac{1}{2}(\gamma_1+\gamma_2)$.

The shape of the distribution shown in Fig. 1(c) has a strong effect on the moments of v_r. For bidisperse suspensions, the plateau of $\varrho(v_r,r)$ ($r<r_c$ and $|v_r|<v_c$) yields an r^{d-1} contribution to the moments $\langle|v_r|^p\rangle$, just as the caustic contribution for identical particles [23]. For $\overline{\mathrm{St}}\ll 1$, when caustics are rare, the dominant contribution to the moments of v_r at small r comes from the plateau of the distribution. But for $\overline{\mathrm{St}}\sim 1$, caustics are abundant and for $p\gtrsim 1$ the moments $\langle|v_r|^p\rangle$ are dominated by the tails of the distribution.

The plateau of the bidisperse distribution below r_c and v_c affects the tails indirectly. Comparing the normalized mono- and bidisperse distributions we see that the tails for $\theta\neq 0$ must lie above those for $\theta=0$. This means that the moments $\langle|v_r|^p\rangle$ must have a minimum for $\theta=0$ (at fixed $\overline{\mathrm{St}}$ and fixed small separation). This is consistent with the findings of Refs. [24–28].

III. ANALYSIS OF THE WHITE-NOISE LIMIT

We now show that all of the above observations can be explained qualitatively by analyzing a one-dimensional white-noise model for the dynamics of a pair of particles. A particle pair in one dimension is described by the four coordinates (x_1,v_1) and (x_2,v_2). It is convenient to transform to the relative coordinates $\Delta x=x_2-x_1$, $\Delta v=v_2-v_1$, $\bar{x}=\frac{1}{2}(x_1+x_2)$, and $\bar{v}=\frac{1}{2}(v_1+v_2)$. At small spatial separations, we can linearize the flow field: $u(x_2,t)-u(x_1,t)\sim A(t)\Delta x$. The spatial dependence in $A(x,t)\equiv\partial_x u(x,t)$ is neglected here. This disregards preferential sampling which is absent in the white-noise limit [1]. The gradient $A(t)$ has zero mean and correlation function $\langle A(t_1)A(t_2)\rangle=3(u_0/\eta)^2\exp(-|t_2-t_1|/\tau)$. For $\theta\neq 0$ there is an additional stochastic driving, $u(x_1,t)+u(x_2,t)\sim 2u(\overline{x},t)$. Neglecting the spatial dependence we write $B(t)\equiv 2u(\overline{x},t)$. The two noise terms $A(t)$ and $B(t)$ are uncorrelated, and $\langle B(t_1)B(t_2)\rangle=4u_0^2\exp(-|t_2-t_1|/\tau)$. We use the de-dimensionalization $\tilde{t}\equiv t\overline{\gamma}$, $\tilde{x}\equiv x/\eta$, $\tilde{v}\equiv v/(\eta\overline{\gamma})$, $\tilde{u}\equiv u/(\eta\overline{\gamma})$. Dropping the tildes we find

$$\frac{d}{dt}\Delta x=\Delta v\quad\text{and}\quad\frac{d}{dt}\begin{bmatrix}\Delta v\\ 2\overline{v}\end{bmatrix}=\begin{bmatrix}1 & \theta\\ \theta & 1\end{bmatrix}\begin{bmatrix}A(t)\Delta x-\Delta v\\ B(t)-2\overline{v}\end{bmatrix}. \quad (2)$$

Note that the equation for $\bar{x}$ decouples and is not considered here. The white-noise limit is taken by letting $\overline{\mathrm{St}}\to\infty$ and $\mathrm{Ku}\to 0$ such that $\overline{\varepsilon}^2\equiv 3\mathrm{Ku}^2\,\overline{\mathrm{St}}$ stays finite. In this limit we obtain $\langle A(t_1)A(t_2)\rangle=\frac{3}{4}\langle B(t_1)B(t_2)\rangle=2\overline{\varepsilon}^2\delta(t_2-t_1)$. The white-noise parameter $\overline{\varepsilon}$ is a measure for the degree of inertia in the problem (2) and plays a similar role as $\overline{\mathrm{St}}$ [1] in the two-dimensional system described above. We are thus left with three coupled dynamical variables, Δx and Δv as in the monodisperse case, and the mean velocity $\overline{v}$. We write $\varrho(\Delta v,\Delta x)\equiv\int d\overline{v}\,P(\Delta v,\Delta x,\overline{v})$, where $P(\Delta v,\Delta x,\overline{v})$ is the steady-state distribution of Δv, Δx, and $\overline{v}$.

A. Crossover scales

In the equation for Δv, Eq. (2), we identify three competing terms: the two noise terms $V_1\equiv A\Delta x$ and $V_2\equiv\theta(B-2\overline{v})$, and the damping term $-\Delta v$:

$$\frac{d}{dt}\Delta v=\underbrace{-\Delta v}_{\text{damping}}+\underbrace{A(t)\Delta x}_{V_1}+\underbrace{\theta(B(t)-2\overline{v})}_{V_2}. \quad (3)$$

The multiplicative-noise term V_1 together with the damping term leads to the power-law tails of the relative-velocity distribution in monodisperse suspensions [7]. The additive-noise term V_2 is proportional to θ and contains the Gaussian white noise $B(t)$, responsible for diffusive behavior at small scales.

Consider first how to estimate r_c. Since the relative strength of V_1 and V_2 depends on Δx, we expect that r_c corresponds to the value of Δx for which V_1 and V_2 are of comparable intensity. We define the noise intensity Φ_X as $\Phi_X\equiv\int_{-1}^{1}dt\,\langle X(t)X(0)\rangle$. Demanding $\Phi_{V_1}\sim\Phi_{V_2}$ yields the estimate

$$r_c\sim\sqrt{\frac{\Phi_{V_2}}{\Phi_A}}\propto\theta. \quad (4)$$

This linear dependence upon θ is consistent with the conclusions of Refs. [11,12], and it is confirmed by the two-dimensional numerical data in Fig. 1(b) (green $\square$). It must be emphasized, however, that the estimate is not precise enough to explain a weak $\overline{\varepsilon}$ dependence that we observe in our numerical simulations of the one-dimensional model (not shown).

Let us now find an estimate for the new crossover scale v_c. To this end we consider small separations and small relative velocities, so that $\Phi_{V_1}\ll\Phi_{V_2}$. This allows us to neglect the term $A(t)\Delta x$ in Eq. (2). The resulting closed set of equations for

$\boldsymbol{v} \equiv [\Delta v, 2\bar{v}]$ gives rise to a Gaussian steady-state distribution

$$\lim_{\Delta v, \Delta x \to 0} P(\Delta v, \Delta x, \bar{v}) \propto \mathrm{e}^{-(1/2)\boldsymbol{v}^T \mathbb{M} \boldsymbol{v}}, \tag{5a}$$

$$\mathbb{M} = \frac{3}{2\bar{\varepsilon}^2(1-\theta^2)} \begin{bmatrix} \frac{2-\theta^2}{\theta^2} & -\frac{1}{\theta} \\ -\frac{1}{\theta} & 1 \end{bmatrix}. \tag{5b}$$

From Eqs. (5) we derive the marginal distribution of Δv and estimate v_c^2 by its variance. This leads to a linear dependence of v_c on both $\bar{\varepsilon}$ and θ:

$$v_c \propto \bar{\varepsilon}\theta. \tag{6}$$

In Fig. 1(b) (red ○), we observe excellent agreement of the two-dimensional numerical data with the linear θ dependence predicted by Eq. (6). The linear dependence on $\bar{\varepsilon}$ was also confirmed in statistical-model simulations but is not shown.

Finally, consider the case where $\Phi_{V_1} \gg \Phi_{V_2}$, that is, either $|\Delta x| \gg r_c$ or $|\Delta v| \gg v_c$. In this limit the dynamics is essentially that of monodisperse suspensions, but with mean Stokes number $\overline{\mathrm{St}}$. For $|\Delta x| \gg r_c$ or $|\Delta v| \gg v_c$ the distribution is therefore expected to show the same power-law tails as the monodisperse case [Fig. 1(c)], with exponent μ_c that depends on $\overline{\mathrm{St}}$.

B. Power-law tails

It follows from the analysis above that the relative dynamics is diffusive for $|\Delta x| \ll r_c$ and $|\Delta v| \ll v_c$. In this case $P(\Delta v, \Delta x, \bar{v})$ is given by the Gaussian distribution (5). In the tails, i.e., for $|\Delta x| \gg r_c$ or $|\Delta v| \gg v_c$, by contrast, the dynamics is that of the monodisperse suspension and we can decompose the joint distribution according to $P(\Delta v, \Delta x, \bar{v}) = \varrho_0(\Delta v, \Delta x) p(\bar{v}) + \delta P(\Delta v, \Delta x, \bar{v})$. Here, $\varrho_0(\Delta v, \Delta x)$ equals the distribution for monodisperse particles ($\theta = 0$) and $\delta P(\Delta x, \Delta v, \bar{v})$ is negligible sufficiently far out in the tails. In order to find $\varrho_0(\Delta x, z)$ we follow Ref. [7] and make the separation ansatz $\varrho_0(\Delta x, z) = \sum_\mu a_\mu g_\mu(\Delta x) Z_\mu(z)$ with $z \equiv \Delta v/\Delta x$ and expansion coefficients a_μ. Inserting this ansatz into the Fokker-Planck equation corresponding to Eq. (2) we obtain

$$g_\mu(\Delta x) = |\Delta x|^{\mu - 1} \quad \text{and} \quad \frac{d}{dz}\left(z + z^2 + \bar{\varepsilon}^2 \frac{d}{dz}\right) Z_\mu = \mu z Z_\mu. \tag{7}$$

This is the equation for a suspension of identical particles [7] with Stokes number $\overline{\mathrm{St}}$. In a slightly different form, Eq. (7) was used to model the effect of wall collisions in turbulent suspensions [29].

Particle-exchange symmetry [7] requires that $Z_\mu(z)$ is symmetric for large $|z|$, $\lim_{z\to\infty} Z_\mu(z)/Z_\mu(-z) = 1$. Numerical analysis shows that Eq. (7) exhibits a discrete set of such solutions [15]. For small $\bar{\varepsilon}$ only two values are allowed: $\mu = 0$ and $\mu = \mu_c(\bar{\varepsilon})$.

In the monodisperse case, $\mu_c(\bar{\varepsilon})$ equals D_2 for $\bar{\varepsilon} > \bar{\varepsilon}_c$. For $\bar{\varepsilon} < \bar{\varepsilon}_c$, by contrast, particle paths coalesce exponentially [30], there is no power-law steady state, and $\mu_c(\bar{\varepsilon})$ becomes negative and loses its meaning as correlation dimension. As a consequence the distribution $g_{\mu_c}(\Delta x) = |\Delta x|^{\mu_c - 1}$ is not normalizable for $\mu_c \leqslant 0$.

In the bidisperse case, this divergence is regularized since diffusion dominates for $|\Delta x| \ll r_c$ and $|\Delta v| \ll v_c$. Thus a power-law steady-state distribution is obtained, even for $\bar{\varepsilon} < \bar{\varepsilon}_c$. This is analogous to the effect of small-scale diffusion that regularizes the power-law steady-state distribution of separations [31].

The full solution of (7) consists of a sum of two terms, $a_0|\Delta x|^{-1} Z_0(z) + a_{\mu_c}|\Delta x|^{\mu_c - 1} Z_{\mu_c}(z)$. As was discussed in [7], the separation ansatz for $\varrho(\Delta x, z)$ is strictly valid only for $|\Delta x| \ll 1$. The term that contains a_0 is therefore subdominant for $\mu_c < 0$. For $\mu_c > 0$ we expect $a_0 \sim \theta \ll a_{\mu_c}$ since a_0 must vanish in order for the distribution to be normalizable over $\Delta x = 0$ as $\theta \to 0$, consistent with the numerical small-θ results in Fig. 2(a). Therefore we disregard the $\mu = 0$ term for all values of $\bar{\varepsilon}$.

Figure 2(b) shows that for $\theta \ll 1$ the exponents of both the Δx and Δv distributions (symbols) equal the numerically calculated $\mu_c(\bar{\varepsilon})$ (solid blue line). The asymptote $Z_{\mu_c}(z) \sim |z|^{\mu_c - 2}$ for large $|z|$ gives rise to the power-law tails in the relative-velocity distribution of the form $|\Delta v|^{\mu_c - 2}$. In d spatial dimensions a similar argument yields tails of the form $v_r^{\mu_c - d - 1}$. This explains the power laws observed in Figs. 1(c) and 2(a).

In summary, the white-noise analysis qualitatively explains not only the existence of the plateau in the relative-velocity distribution and the corresponding crossover scales r_c and v_c, it also yields the linear dependence of these scales upon θ, and explains the power-law tails. Thus, the one-dimensional white-noise analysis qualitatively explains all the important features in Fig. 1.

C. Failure of perturbation theory in $\bar{\varepsilon}$

Figure 2(b) demonstrates that the exponent μ_c depends very sensitively on $\bar{\varepsilon}$, for small $\bar{\varepsilon}$. Here we show that this dependence is nonanalytic. This means that it cannot be obtained by perturbation theory in $\bar{\varepsilon}$, and this in turn is a likely reason [32] why Borel resummation of perturbation theory does not yield accurate results for the correlation dimension D_2 (Fig. 1 in Ref. [33]). There is, to date, no theory explaining these observations.

The exponent μ_c appears as a generalized eigenvalue in Eq. (7), but exact solutions to Eq. (7) are known only for $\mu = 0$ [30], $\mu = -1$ [34], and in the large $\bar{\varepsilon}$ limit [35]. The physical solution at small $\bar{\varepsilon}$ corresponds to the eigenvalue $\mu_c(\bar{\varepsilon})$. The solution for $\mu = -1$ is unphysical since it does not obey particle-exchange symmetry.

Numerical analysis reveals that $\mu_c(\bar{\varepsilon}) \to -1$ as $\bar{\varepsilon} \to 0$. We write $\mu_c = -1 + \delta\mu$, where $\delta\mu \geqslant 0$ is an "eigenvalue splitting" that vanishes as $\bar{\varepsilon} \to 0$, and attempt to find the physical solution by perturbation theory in $\delta\mu$:

$$Z_{\mu_c}(z) = Z^{(0)}(z) + \delta\mu\, Z^{(1)}(z) + \delta\mu^2 Z^{(2)}(z) + \ldots. \tag{8}$$

Substituting (8) into (7) we obtain a hierarchy of differential equations for $Z^{(n)}$ given by

$$\frac{d}{dz}\left[z + z^2 + \bar{\varepsilon}^2 \frac{d}{dz}\right] Z_\mu^{(0)} + z Z_\mu^{(0)} = 0, \tag{9a}$$

$$\frac{d}{dz}\left[z + z^2 + \bar{\varepsilon}^2 \frac{d}{dz}\right] Z_\mu^{(n)} + z Z_\mu^{(n)} = z Z_\mu^{(n-1)}, \quad n \geqslant 1. \tag{9b}$$

Equation (9a) is solved by the unphysical solution discussed above, i.e., $Z^{(0)} = Z_{-1}$. The general form of the latter is known [34]:

$$Z_{-1} = C_1(z+1)e^{-U(z)} + C_2(z+1)\int_{-\infty}^{z} \mathrm{d}t\, \frac{e^{U(t)-U(z)}}{(t+1)^2}. \tag{10}$$

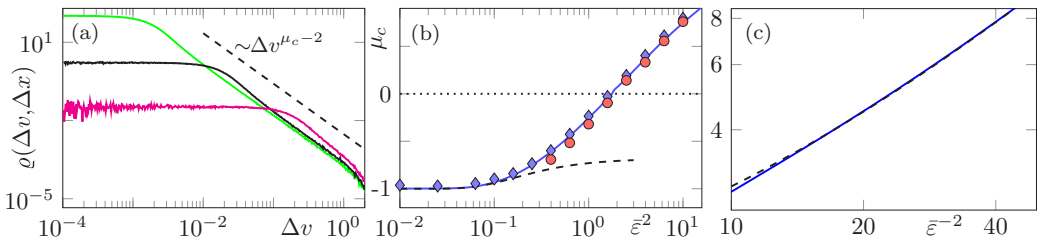

FIG. 2. (a) Distribution of Δv at small Δx from white-noise simulations of Eq. (2), for $\bar{\varepsilon}^2 = 2$ and $\theta = 10^{-3}$, $\theta = 10^{-2}$, and $\theta = 10^{-1}$; green, black, and pink curves, respectively. (b) Exponent μ_c as a function of $\bar{\varepsilon}$ from simulations of Eq. (2) for $\theta = 0.01$, obtained from fit to Δx tails (blue $\Diamond$), and from fit to Δv tails (red $\circ$). Result for equal St obtained by numerical solution of Eq. (7) (solid blue line) and the analytical prediction, Eq. (12) (dashed black line). (c) Same data as for the solid and dashed lines in panel (b), but plotted here as $-\log(1+\mu_c)$ versus $\bar{\varepsilon}^{-2}$.

Here $U(z) \equiv (\frac{1}{3}z^3 + \frac{1}{2}z^2)/\bar{\varepsilon}^2$, and C_1 and C_2 are constants. The first-order solution reads

$$Z^{(1)} = \frac{z+1}{\bar{\varepsilon}^2}\int_{-\infty}^{z} dt\, \frac{e^{U(t)-U(z)}}{(t+1)^2}\int_{-1}^{t} dt' t'(t'+1)Z_{-1}(t'). \quad (11)$$

The integrand involves Z_{-1}, and we must take $C_1 = 0$ in Eq. (10) for Z_{-1} since the first term in (10) is not normalizable. We further choose $C_2 = -\bar{\varepsilon}^2$ because it normalizes the large-z tails of Z_{-1} to $Z_{-1} \sim -z^{-3}$. To evaluate (11) we use the fact that $\delta\mu \to 0$ as $\bar{\varepsilon} \to 0$ and apply a WKB approximation [36] of Z_{-1} that becomes exact in the limit $\bar{\varepsilon} \to 0$. The equation for Z_{-1} has two "turning points" at $z = -1,0$ where the WKB approximation breaks down. We find locally exact solutions and use these to match the WKB solutions across the turning points. Details of this asymptotic-matching method are given in the Supplemental Material [37]. In this way we find $Z^{(1)} \sim |z|^{-3}\log|z|$ for large negative values of z, and $Z^{(1)} \sim |z|^{-3}[2\pi e^{1/(6\bar{\varepsilon}^2)} - \log|z|]$ for large positive z. Imposing particle-exchange symmetry yields

$$\mu_c \sim -1 + \delta\mu \quad \text{with} \quad \delta\mu = \pi^{-1}\exp[-1/(6\bar{\varepsilon}^2)]. \quad (12)$$

The splitting $\delta\mu$ is shown as a dashed black line in Figs. 2(b) and 2(c). It agrees with the numerical data for μ_c (blue) for small $\bar{\varepsilon}^2$ but breaks down for $\bar{\varepsilon}^2 \approx 0.1$.

We emphasize that the nonanalytic dependence (12) cannot be obtained by the $\bar{\varepsilon}$-perturbation theory described in Refs. [1,38,39]. That approach starts by rescaling $z \to \bar{\varepsilon}z$, and solves the resulting equation $\frac{d}{dz}(z + \bar{\varepsilon}z^2 + \frac{d}{dz})Z_\mu = \bar{\varepsilon}\mu z Z_\mu$ perturbatively in $\bar{\varepsilon}$. The solution remains essentially Gaussian. Even for very small $\bar{\varepsilon}$, however, the z dynamics can escape from $z \approx 0$ to $-\infty$ by forming caustics [1]. This gives rise to power-law tails that are not described by perturbation theory. Higher orders in $\bar{\varepsilon}$ improve the accuracy only locally, inside an $\bar{\varepsilon}$-sized "boundary layer" [40] around $z = 0$, but not in the tails. Consequently, perturbation theory fails to give the nonanalytical dependence (12) since all perturbative corrections to $\mu_c \sim -1$ vanish [32].

Our theory, by contrast, provides a uniform approximation valid for small $\bar{\varepsilon}$ and arbitrary z. It allows one to compute the exponentially small eigenvalue splitting $\delta\mu$ because it captures the formation of caustics. For small $\bar{\varepsilon}$, the rate J of caustic formation is $J \sim (2\pi)^{-1}e^{-1/6\bar{\varepsilon}^2}$ [1]. It follows that $\mu_c \sim 2J - 1$ at small $\bar{\varepsilon}$.

We now show that caustics cause similar problems in small-St expansions [1,11,41–44]. In one dimension, the equation for z reads in dimensional units

$$\frac{d}{dt}z = -\gamma z - z^2 + \gamma A(x,t). \quad (13)$$

The Stokes number used in DNS of heavy particles in turbulence [45,46] is $\kappa \equiv u_0/(\eta\gamma)$ [1]. We take A in Eq. (13) to be constant. In this "persistent limit" the local fluid-velocity gradients are roughly constant during the time η/u_0 [1]. As $\kappa \to 0$ we find that $z \sim A$, with distribution $P(A) = (6\pi u_0^2/\eta^2)^{-1/2}\exp[-A^2/(6u_0^2/\eta^2)]$, localized around zero. As in the white-noise case, this local approximation fails when caustics allow z to escape to $-\infty$. Kramers-escape theory for weak colored noise [47,48] reveals that caustics occur in the persistent limit when $A < -\gamma/4$, with probability $p = \int_{-\infty}^{-\gamma/4} dA\, P(A)$. Evaluating this integral for $\kappa \ll 1$, one obtains a nonanalytic dependence, $p \propto \exp[-1/(96\kappa^2)]$, consistent with Ref. [49]. In DNS a similar nonanalytic dependence is found [50], albeit of a slightly different form because the turbulent velocity gradients are non-Gaussian. We conclude that the perturbation theories in the white-noise limit and in time-correlated flows fail for the same reason. Both expansions are valid only locally near $z = 0$ and do not accommodate caustics.

IV. CONCLUSIONS

We analyzed the distribution of relative velocities in turbulence between small, heavy particles with different Stokes numbers St. We demonstrated that the difference in St causes diffusive relative motion at small separations, giving rise to a plateau in the distribution for relative velocities smaller than a cut off v_c. This is in qualitative agreement with DNS [51]. Figure 2 in Ref. [51] shows the v_r distribution for a bidisperse suspension. The cut off v_c depends linearly on both θ, the parameter characterizing the difference in Stokes numbers, and $\bar{\varepsilon}$, which is a measure for the mean Stokes number of the system. At small values of θ and $\bar{\varepsilon}$ the distribution exhibits algebraic tails $|v_r|^{\mu_c - d - 1}$ as in the monodisperse case. The exponent μ_c is determined by the phase-space correlation dimension of a monodisperse system with mean Stokes number $\overline{\mathrm{St}}$. When $\overline{\mathrm{St}}$ is $\mathcal{O}(1)$ or larger, the moments of relative velocities at small separations are dominated by the tails of the distribution. As the parameters θ and $\bar{\varepsilon}$ become larger, both our simulations and the analysis of the white-noise model show that the tails gradually disappear, making space

for the diffusive (Gaussian) behavior below $v_c \propto \overline{\varepsilon}\,\theta$. The DNS of Ref. [51] are for quite large θ and $\overline{\varepsilon}$. It would be of interest to perform DNS for smaller parameter values to find the power-law tails we predict here.

Our analysis shows how sensitive the distribution is to polydispersity. This is important for experiments tracking the dynamics of micrometer-size particles in turbulence [9], where strict monodispersity is difficult to achieve.

We explained these observations by analyzing a one-dimensional statistical model in the white-noise limit. The difference in Stokes numbers regularizes the distribution, so that the bidisperse model has a power-law steady state at small $\overline{\varepsilon}$. This makes it possible to compute how the power-law exponent μ_c depends on the inertia parameter $\overline{\varepsilon}$. We demonstrated that the dependence of μ_c upon $\overline{\varepsilon}$ is not analytic.

Our theory explains why small-$\overline{\varepsilon}$ expansions fail to give nonanalytic contributions to physical quantities in the white-noise limit. It is likely that nonanalytic terms in white-noise expansions for the correlation dimension [32] and Lyapunov exponents [38,39] in two and three dimensions have similar origins, and we speculate that Eqs. (12) are only the first two terms in an infinite series of the form $\sum_{k=0}^{\infty} e^{-k/(6\overline{\varepsilon}^2)} \sum_{m=0}^{\infty} b_m^{(k)} \overline{\varepsilon}^{2m}$ [52], possibly also containing logarithmic terms, $\log^n \overline{\varepsilon}^2$.

We remark that the analysis of μ_c in the one-dimensional white-noise model is special insofar as its conventional perturbation expansion vanishes exactly [32], as mentioned above. This renders the nonanalytic correction (12) leading. In higher dimensions this is, however, not the case. We therefore expect perturbation theory to fail in these cases only when the nonanalytical terms become comparable to the perturbative ones. The Borel sum for the correlation dimension in two dimensions, for instance, fails only at $\overline{\varepsilon} \approx 0.1$ [32] where $\overline{\varepsilon}^2 \approx e^{-1/(6\overline{\varepsilon}^2)}$.

More generally we explained that small-St expansions for heavy particles in turbulence [1,11,41–44] suffer from similar problems when caustics occur. This indicates that matched asymptotic expansions (or similar methods) are required to explain the characteristic minimum [46] of the correlation dimension as a function of St.

Our predictions can be directly tested by experiments or by DNS of turbulent bidisperse turbulent suspensions. We note, however, that our analysis pertains to the dynamics in the dissipative range. At higher Stokes numbers, when separations between particle pairs explore the inertial range [53,54], we expect corrections to the power-law exponents derived here. Furthermore, strong intermittency is expected to increase the rate of caustic formation for heavy particles in turbulent flows. This could imply that the breakdown of perturbation theory for heavy particles in turbulent flows is perhaps even more pronounced than predicted by our model calculations.

ACKNOWLEDGMENTS

This work was supported by Vetenskapsrådet (Grant No. 2013-3992), Formas (Grant No. 2014-585), and by the grant "Bottlenecks for particle growth in turbulent aerosols" from the Knut and Alice Wallenberg Foundation, Dnr. KAW 2014.0048. The numerical computations used resources provided by C3SE and SNIC.

[1] K. Gustavsson and B. Mehlig, Statistical models for spatial patterns of heavy particles in turbulence, Adv. Phys. **65**, 1 (2016).

[2] S. Sundaram and L. R. Collins, Collision statistics in an isotropic particle-laden turbulent suspension, J. Fluid. Mech. **335**, 75 (1997).

[3] G. Falkovich, A. Fouxon, and G. Stepanov, Acceleration of rain initiation by cloud turbulence, Nature (London) **419**, 151 (2002).

[4] M. Wilkinson and B. Mehlig, Caustics in turbulent aerosols, Europhys. Lett. **71**, 186 (2005).

[5] M. Wilkinson, B. Mehlig, and V. Bezuglyy, Caustic Activation of Rain Showers, Phys. Rev. Lett. **97**, 048501 (2006).

[6] J. Bec, L. Biferale, M. Cencini, A. Lanotte, and F. Toschi, Intermittency in the velocity distribution of heavy particles in turbulence, J. Fluid Mech. **646**, 527 (2010).

[7] K. Gustavsson and B. Mehlig, Distribution of relative velocities in turbulent aerosols, Phys. Rev. E **84**, 045304 (2011).

[8] J. P. L. C. Salazar and L. R. Collins, J. Fluid Mech. **696**, 45 (2012).

[9] G. P. Bewley, E. W. Saw, and E. Bodenschatz, New J. Phys. **15**, 083051 (2013).

[10] V. Perrin and H. Jonker, Relative velocity distribution of inertial particles in turbulence: A numerical study, Phys. Rev. E **92**, 043022 (2015).

[11] J. Chun, D. L. Koch, S. L. Rani, A. Ahluwalia, and L. R. Collins, Clustering of aerosol particles in isotropic turbulence, J. Fluid Mech. **536**, 219 (2005).

[12] J. Bec, A. Celani, M. Cencini, and S. Musacchio, Clustering and collisions in random flows, Phys. Fluids **17**, 073301 (2005).

[13] M. Wilkinson, B. Mehlig, and V. Uski, Stokes trapping and planet formation, Astrophys. J. Suppl. **176**, 484 (2008).

[14] F. Windmark, T. Birnstiel, C. W. Ormel, and C. P. Dullemond, Breaking through: The effects of a velocity distribution on barriers of dust growth, Astron. Astrophys. **544**, L16 (2012).

[15] K. Gustavsson and B. Mehlig, Relative velocities of inertial particles in turbulent aerosols, J. Turbulence **15**, 34 (2014).

[16] A. Pumir and M. Wilkinson, Collisional aggregation due to turbulence, Ann. Rev. Condens. Matter Phys. **7**, 141 (2016).

[17] J. Schumacher, J. D. Scheel, D. Krasnov, D. A. Donzis, V. Yakhot, and K. R. Sreenivasan, Small-scale universality in fluid turbulence, Proc. Natl. Acad. Sci. USA **111**, 10961 (2014).

[18] K. Gustavsson, S. Vajedi, and B. Mehlig, Clustering of Particles Falling in a Turbulent Flow, Phys. Rev. Lett. **112**, 214501 (2014).

[19] J. Bec, H. Homann, and S. S. Ray, Gravity-Driven Enhancement of Heavy Particle Clustering in Turbulent Flow, Phys. Rev. Lett. **112**, 184501 (2014). .

[20] P. J. Ireland, A. D. Bragg, and L. R. Collins, The effect of Reynolds number on inertial particle dynamics in isotropic turbulence. Part 2. Simulations with gravitational effects, J. Fluid Mech. **796**, 659 (2016).

[21] V. Mathai, E. Calzavarini, J. Brons, C. Sun, and D. Lohse, Microbubbles and Microparticles are Not Faithful Tracers of Turbulent Acceleration, Phys. Rev. Lett. **117**, 024501 (2016).

[22] H. Parishani, O. Ayala, B. Rosa, L.-P. Wang, and W. W. Grabowski, Effects of gravity on the acceleration and pair statistics of inertial particles in homogeneous isotropic turbulence, Phys. Fluids **27**, 033304 (2015).

[23] K. Gustavsson, E. Meneguz, M. Reeks, and B. Mehlig, Inertial-particle dynamics in turbulent flows: Caustics, concentration fluctuations, and random uncorrelated motion, New J. Phys. **14**, 115017 (2012).

[24] H. J. Völk, F. C. Jones, G. E. Morfill, and S. Röser, Collisions between grains in a turbulent gas, Astron. Astrophys. **85**, 316 (1980).

[25] H. Mizuno, W. J. Markiewicz, and H. J. Völk, Grain growth in turbulent protoplanetary accretion disks, Astron. Astrophys. **195**, 183 (1988).

[26] W. J. Markiewicz, H. Mizuno, and H. J. Völk, Turbulence induced relative velocity between two grains, Astron. Astrophys. **242**, 286 (1991).

[27] L. Pan, P. Padoan, and J. Scalo, Turbulence induced relative velocity of dust particles. The bidisperse case, Astrophys. J. **791**, 48 (2014).

[28] M. James and S. S. Ray, Enhanced droplet collision rates and impact velocities in turbulent flows: The effect of polydispersity and transient phases, Sci. Rep. **7**, 12231 (2017); see also arXiv:1603.05880

[29] S. Belan, I. Fouxon, and G. Falkovich, Localization-Delocalization Transitions in Turbophoresis of Inertial Particles, Phys. Rev. Lett. **112**, 234502 (2014).

[30] M. Wilkinson and B. Mehlig, Path coalescence transition and its applications, Phys. Rev. E **68**, 040101 (2003).

[31] M. Wilkinson, R. Guichardaz, M. Pradas, and A. Pumir, Power-law distributions in noisy dynamical systems, Europhys. Lett. **111**, 50005 (2015).

[32] K. Gustavsson, B. Mehlig, and M. Wilkinson, Analysis of the correlation dimension of inertial particles, Phys. Fluids **27**, 073305 (2015).

[33] M. Wilkinson, B. Mehlig, and K. Gustavsson, Correlation dimension of inertial particles in random flows, Europhys. Lett. **89**, 50002 (2010).

[34] S. A. Derevyanko, G. Falkovich, K. Turitsyn, and S. Turitsyn, Lagrangian and Eulerian descriptions of inertial particles in random flows, J. Turbulence **8**, N16 (2007).

[35] H. Schomerus and M. Titov, Phys. Rev. E **66**, 066207 (2002).

[36] C. M. Bender and S. A. Orszag, *Advanced mathematical methods for scientists and engineers* (McGraw-Hill, New York, 1978).

[37] See Supplemental Material at http://link.aps.org/supplemental/10.1103/PhysRevE.96.061102 for additional details on the derivation of Eq. (11) and for a description of how to obtain the WKB solution for $Z_{-1}(z)$ that is used to obtain Eq. (12).

[38] B. Mehlig and M. Wilkinson, Coagulation by Random Velocity Fields as a Kramers Problem, Phys. Rev. Lett. **92**, 250602 (2004).

[39] K. Duncan, B. Mehlig, S. Östlund, and M. Wilkinson, Clustering in Mixing Flows, Phys. Rev. Lett. **95**, 240602 (2005).

[40] E. J. Hinch, *Perturbation methods* (Cambridge University Press, Cambridge, 1991).

[41] M. R. Maxey, The gravitational settling of aerosol particles in homogeneous turbulence and random flow fields, J. Fluid Mech. **174**, 441 (1987).

[42] T. Elperin, N. Kleeorin, and I. Rogachevskii, Self-Excitation of Fluctuation of Inertial Particle Concentration in Turbulent Fluid Flow, Phys. Rev. Lett. **77**, 5373 (1996).

[43] E. Balkovsky, G. Falkovich, and A. Fouxon, Intermittent Distribution of Inertial Particles in Turbulent Flows, Phys. Rev. Lett. **86**, 2790 (2001).

[44] M. Wilkinson, B. Mehlig, S. Östlund, and K. P. Duncan, Unmixing in random flows, Phys. Fluids **19**, 113303 (2007).

[45] J. Bec, L. Biferale, G. Boffetta, M. Cencini, S. Musacchio, and F. Toschi, Lyapunov exponents of heavy particles in turbulence, Phys. Fluids **18**, 091702 (2006).

[46] J. Bec, L. Biferale, M. Cencini, A. Lanotte, S. Musacchio, and F. Toschi, Heavy Particle Concentration in Turbulence at Dissipative and Inertial Scales, Phys. Rev. Lett. **98**, 084502 (2007).

[47] G. P. Tsironis and P. Grigolini, Color-Induced Transition to a Nonconventional Diffusion Regime, Phys. Rev. Lett. **61**, 7 (1988).

[48] A. J. Bray and A. J. McKane, Instanton Calculation of the Escape Rate for Activation over a Potential Barrier Driven by Colored Noise, Phys. Rev. Lett. **62**, 493 (1989).

[49] K. Gustavsson and B. Mehlig, Distribution of velocity gradients and rate of caustic formation in turbulent aerosols at finite Kubo numbers, Phys. Rev. E **87**, 023016 (2013).

[50] G. Falkovich and A. Pumir, Sling effect in collisions of water droplets in turbulent clouds, J. Atmos. Sci. **64**, 4497 (2007).

[51] L. Pan, P. Padoan, and J. Scalo, Turbulence-induced relative velocity of dust particles. III. The probability distribution, Astrophys. J. **792**, 69 (2014).

[52] G. Dorigoni, An introduction to resurgence, trans-series and alien calculus, arXiv:1411.3585.

[53] B. Mehlig, M. Wilkinson, and V. Uski, Colliding particles in highly turbulent flows, Phys. Fluids **19**, 098107 (2007).

[54] K. Gustavsson, B. Mehlig, M. Wilkinson, and V. Uski, Variable-Range Projection Model for Turbulence-Driven Collisions, Phys. Rev. Lett. **101**, 174503 (2008).